Fundamental limit of nanophotonic light trapping in solar cells

Zongfu Yu[1], Aaswath Raman, and Shanhui Fan[1]

Ginzton Laboratory, Stanford University, Stanford, CA 94305

Edited* by David A. B. Miller, Stanford University, Stanford, CA, and approved August 13, 2010 (received for review June 11, 2010)

Establishing the fundamental limit of nanophotonic light-trapping schemes is of paramount importance and is becoming increasingly urgent for current solar cell research. The standard theory of light trapping demonstrated that absorption enhancement in a medium cannot exceed a factor of $4n^2/\sin^2\theta$, where n is the refractive index of the active layer, and θ is the angle of the emission cone in the medium surrounding the cell. This theory, however, is not applicable in the nanophotonic regime. Here we develop a statistical temporal coupled-mode theory of light trapping based on a rigorous electromagnetic approach. Our theory reveals that the conventional limit can be substantially surpassed when optical modes exhibit deep-subwavelength-scale field confinement, opening new avenues for highly efficient next-generation solar cells.

The ultimate success of photovoltaic (PV) cell technology requires great advancements in both cost reduction and efficiency improvement. An approach that simultaneously achieves these two objectives is to use light-trapping schemes. Light trapping allows cells to absorb sunlight using an active material layer that is much thinner than the material's intrinsic absorption length. This effect then reduces the amount of materials used in PV cells, which cuts cell cost in general, and moreover facilitates mass production of PV cells that are based on less abundant materials. In addition, light trapping can improve cell efficiency, because thinner cells provide better collection of photogenerated charge carriers, and potentially a higher open circuit voltage (1).

The theory of light trapping was initially developed for conventional cells where the light-absorbing film is typically many wavelengths thick (2–4). From a ray-optics perspective, conventional light trapping exploits the effect of total internal reflection between the semiconductor material (such as silicon, with a refractive index $n \sim 3.5$) and the surrounding medium (usually assumed to be air). By roughening the semiconductor–air interface (Fig. 1*A*), one randomizes the light propagation direction inside the material. The effect of total internal reflection results in a much longer propagation distance inside the material and hence a substantial absorption enhancement. For such light-trapping schemes, the standard theory shows that the absorption enhancement factor has an upper limit of $4n^2/\sin^2\theta$ (2–4), where θ is the angle of the emission cone in the medium surrounding the cell. This limit of $4n^2/\sin^2\theta$ will be referred to in this paper as the *conventional limit*. This form is in contrast to the $4n^2$ limit, which strictly speaking is only applicable to cells with isotropic angular response, but is nevertheless quite commonly used in the literature.

For nanoscale films with thicknesses comparable or even smaller than wavelength scale, some of the basic assumptions of the conventional theory are no longer applicable. Whether the conventional limit still holds thus becomes an important open question that is currently being pursued both numerically (5–15) and experimentally (16–23).

In this article, we develop a statistical coupled-mode theory that describes light trapping in general from a rigorous electromagnetic perspective. Applying this theory, we show that the limit of $4n^2/\sin^2\theta$ is only correct in bulk structures. In the nanophotonic regime, the absorption enhancement factor can go far beyond this limit with proper design. As a specific example, we numerically demonstrate a light-trapping scheme, based on subwavelength modal confinement, with an absorption enhancement factor of $12 \times 4n^2$ over a virtually unlimited spectral bandwidth and with near-isotropic angular response. We also show theoretically that, in the absence of subwavelength modal confinement, a grating structure by itself can achieve an enhancement ratio above $4n^2$. Such an enhancement, however, is always associated with a strong angular response. As a result, it is difficult to use grating structures alone to achieve enhancement factors beyond the conventional limit of $4n^2/\sin^2\theta$.

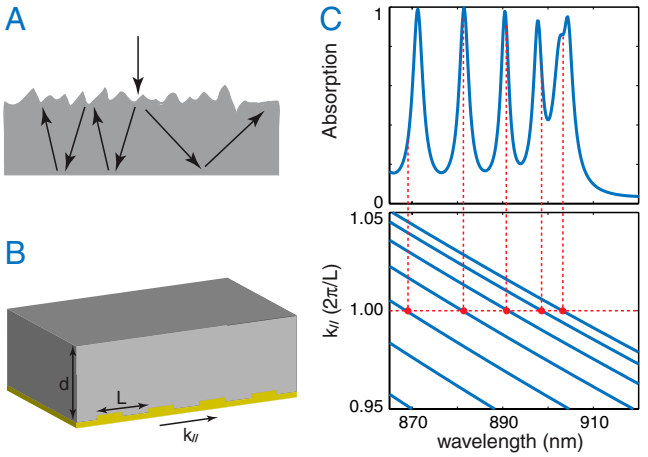

Fig. 1. Light trapping with random texture and a grating structure. (*A*) Light trapping by randomly textured surface. (*B*) Light trapping using a periodic grating on a back-reflector (yellow); $d = 2$ μm, $L = 250$ nm. The depth and width of the dielectric groove in the grating are 50 and 175 nm, respectively. The dielectric material is crystalline silicon. (*C*) Absorption spectrum [transverse magnetic (TM) mode, normal incidence] and dispersion relation of waveguide modes for the structure in *B*. The dispersion relation is approximated as $\omega = \frac{c}{n}[(\frac{m\pi}{d})^2 + k_{//}^2]$, or equivalently in terms of free-space wavelength $\lambda = \frac{2\pi n}{\sqrt{(m\pi/d)^2+k_{//}^2}}$, where $m = 1, 2, 3, \ldots$ is the band index indicating the field variation in the transverse direction. Resonances occur when $k_{//} = 2\pi/L$ (red dots).

Theory

To illustrate our theory, we consider a high-index thin-film active layer with a high-reflectivity mirror at the bottom and air on top. Such a film supports guided optical modes. In the limit where the absorption of the active layer is weak, these guided modes typically have a propagation distance along the film that is much longer than the thickness of the film. Light trapping is accomplished by coupling incident plane waves into these guided

Author contributions: Z.Y. and S.F. designed research; Z.Y., A.R., and S.F. performed research; Z.Y., A.R., and S.F. analyzed data; and Z.Y., A.R., and S.F. wrote the paper.

The authors declare no conflict of interest.

*This Direct Submission article had a prearranged editor.

[1]To whom correspondence may be addressed. E-mail: zfyu@stanford.edu or shanhui@stanford.edu.

This article contains supporting information online at www.pnas.org/lookup/suppl/doi:10.1073/pnas.1008296107/-/DCSupplemental.

modes, with either a grating with periodicity L (Fig. 1*B*) or random Lambertian roughness (Fig. 1*A*). It is well known that a system with random roughness can be understood by taking the $L \to \infty$ limit of the periodic system (10, 24). Thus, we will focus on periodic systems. As long as L is chosen to be sufficiently large, i.e., at least comparable to the free-space wavelength of the incident light, each incident plane wave can couple into at least one guided mode. By the same argument, such a guided mode can couple to external plane waves, creating a guided resonance (25).

A typical absorption spectrum for such a film (6) is reproduced in Fig. 1*C*. The absorption spectrum consists of multiple peaks, each corresponding to a guided resonance. The absorption is strongly enhanced in the vicinity of each resonance. However, compared to the broad solar spectrum, each individual resonance has very narrow spectral width. Consequently, to enhance absorption over a substantial portion of the solar spectrum, one must rely upon a collection of these peaks. Motivated by this observation, we develop a statistical temporal coupled-mode theory that describes the aggregate contributions from all resonances.

We start by identifying the contribution of a single resonance to the total absorption over a broad spectrum. The behavior of an individual guided resonance, when excited by an incident plane wave, is described by the temporal coupled-mode theory equation (26, 27)

$$\frac{d}{dt}a = \left(j\omega_0 - \frac{N\gamma_e + \gamma_i}{2}\right)a + j\sqrt{\gamma_e}S. \qquad [1]$$

Here a is the resonance amplitude, normalized such that $|a|^2$ is the energy per unit area in the film, ω_0 is the resonance frequency, and γ_i is the intrinsic loss rate of the resonance due to material absorption. S is the amplitude of the incident plane wave, with $|S|^2$ corresponding to its intensity. We refer to a plane wave that couples to the resonance as a *channel*. The leakage rate γ_e describes the coupling between the resonance and the channel that carries the incident wave. In general, the grating may phase match the resonance to other plane-wave channels as well. We assume a total of N such channels. Equivalent to the assumption of a Lambertian emission profile as made in ref. 2, we further assume that the resonance leaks to each of the N channels with the same rate γ_e. Under these assumptions, the absorption spectrum of the resonance is (26)

$$A(\omega) = \frac{\gamma_i\gamma_e}{(\omega-\omega_0)^2 + (\gamma_i + N\gamma_e)^2/4}. \qquad [2]$$

For light-trapping purposes, the incident light spectrum is typically much wider than the linewidth of the resonance. For this case, we characterize the contribution of a single resonance to the total absorption by a *spectral cross-section*:

$$\sigma = \int_{-\infty}^{\infty} A(\omega)d\omega. \qquad [3]$$

Notice that spectral cross-section has units of frequency and has the following physical interpretation: For an incident spectrum with bandwidth $\Delta\omega \gg \sigma$, a resonance contributes an additional $\sigma/\Delta\omega$ to the spectrally averaged absorption coefficient.

For a single resonance, from Eqs. **2** and **3**, the spectral cross-section is

$$\sigma = 2\pi\gamma_i \frac{1}{N + \gamma_i/\gamma_e}, \qquad [4]$$

which reaches a maximum value of

$$\sigma_{\max} = \frac{2\pi\gamma_i}{N} \qquad [5]$$

in the *overcoupling* regime when $\gamma_e \gg \gamma_i$. We emphasize that the requirement to operate in the strongly overcoupling regime arises from the need to accomplish broadband absorption enhancement. In the opposite narrowband limit, when the incident radiation is far narrower than the resonance bandwidth, one would instead prefer to operate at the critical coupling condition by choosing $\gamma_i = N\gamma_e$, which results in $(100/N)\%$ absorption at the resonant frequency of ω_0. The use of critical coupling, however, has a lower spectral cross-section and is not optimal for the purpose of broadband enhancement. The intrinsic decay rate γ_i differentiates between the two cases of broadband and narrowband. For light trapping in solar cells, we are almost always in the broadband case where the incident radiation has bandwidth $\Delta\omega \gg \gamma_i$.

We can now calculate the upper limit for absorption by a given medium, by summing over the maximal spectral cross-section of all resonances:

$$A_T = \frac{\sum \sigma_{\max}}{\Delta\omega} = \frac{1}{\Delta\omega}\sum_m \frac{2\pi\gamma_{i,m}}{N}, \qquad [6]$$

where the summation takes place over all resonances (labeled by m) in the frequency range of $[\omega,\omega+\Delta\omega]$. In the overcoupling regime, the peak absorption from each resonance is in fact relatively small; therefore the total cross-section can be obtained by summing over the contributions from individual resonances. In addition, we assume that the medium is weakly absorptive such that single-pass light absorption is negligible.

Eq. **6** is the main result of this paper. In the following discussion, we will first use Eq. **6** to reproduce the well-known $4n^2$ conventional limit, and then consider a few relevant scenarios where the effect of strong light confinement becomes important.

Light-Trapping in Bulk Structures

We first consider a structure with period L and thickness d that are both much larger than the wavelength. In this case, the resonance can be approximated as propagating plane waves inside the bulk structure. Thus, the intrinsic decay rate for each resonance is related to a material's absorption coefficient α_0 by $\gamma_i = \alpha_0\frac{c}{n}$.

The number of resonances in the frequency range $[\omega,\omega+\delta\omega]$ is (28)

$$M = \frac{8\pi n^3\omega^2}{c^3}\left(\frac{L}{2\pi}\right)^2\left(\frac{d}{2\pi}\right)\delta\omega. \qquad [7]$$

Each resonance in the frequency range can couple to channels that are equally spaced by $\frac{2\pi}{L}$ in the parallel wavevector $k_{//}$ space (Fig. 2*A*). Moreover, because each channel is a propagating plane wave in air, its parallel wavevector needs to satisfy $|k_{//}| \le \omega/c$. Thus, the number of channels is

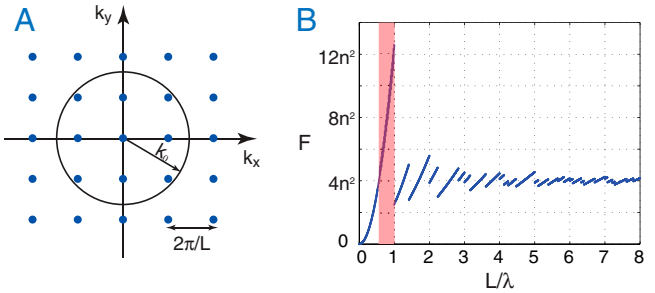

Fig. 2. Light trapping in periodic structures. (*A*) Blue dots represent channels in the k space. Channels in the circle correspond to free-space propagating modes. (*B*) Theoretical upper limit of the absorption enhancement factor using a light-trapping scheme where a square-lattice periodic grating structure is introduced into a thin film. Red area represents a spectral range where the upper limit of the absorption enhancement factor F is above $4n^2$.

$$N = \frac{2\pi\omega^2}{c^2}\left(\frac{L}{2\pi}\right)^2. \quad [8]$$

From Eq. **6**, the upper limit for the absorption coefficient of this system is then

$$A_T = \frac{2\pi\gamma_i}{\Delta\omega}\cdot\frac{M}{N} = 4n^2\alpha_0 d, \quad [9]$$

resulting in the upper limit for the absorption enhancement factor F,

$$F \equiv \frac{A_T}{\alpha_0 d} = 4n^2, \quad [10]$$

which reproduces the $4n^2$ conventional limit, appropriate for the Lambertian emission case with $\sin\theta = 1$. The theory can be generalized to the case of a restricted emission cone and reproduces the standard result of $4n^2/\sin^2\theta$ (*SI Text*).

The analysis here also points to scenarios where the conventional limit is no longer applicable. Eq. **8** is not applicable when the periodicity is comparable to the wavelength, whereas Eq. **7** is not valid when the film thickness is much smaller than the wavelength. Below, we consider both of these cases.

Light-Trapping in Structures with Wavelength-Scale Periodicity

When the periodicity L is comparable to the wavelength λ, the discrete nature of the channels becomes important (Fig. 2*A*). To illustrate this effect, we assume that the film has a high refractive index (for example, silicon), such that the wavelength in the material is small compared with the periodicity. We also assume that the film has a thickness of a few wavelengths. In this case, all modes have approximately the same decay rate $\gamma_i = \alpha_0\frac{c}{n}$, and Eq. **7** can still be used to count the number of resonances.

Using Eq. **6**, for normally incident light, we calculate the upper limit of the absorption enhancement factor as a function of L/λ (Fig. 2*B*) when the structure has a square lattice. The discontinuous changes in Fig. 2*B* correspond to the emergence of new channels. In particular, when $\lambda > L$, there is only a single channel independent of frequency. On the other hand, the number of resonances is frequency dependent. As a result, the maximum enhancement factor increases quadratically as a function of frequency. In order to maximize the absorption, one should choose the periodicity to be slightly smaller than the wavelength range of interest (red region in Fig. 2*B*). We note that the upper limit for the absorption enhancement factor approaches $4n^2$ for a large period, $L \gg \lambda$.

The above analysis can be used to provide considerable insight into the behavior of grating structures. In particular, one expects that a 2D grating structure is superior to a 1D grating, because a 2D grating can provide access to a significantly larger number of resonances. Also, an asymmetric grating profile should be beneficial, because with a symmetric profile there are resonances that cannot be coupled to incident light due to symmetry constraints. These findings are consistent with existing literature (10, 29).

The use of grating structures on a relatively thick film to enhance optical absorption has been extensively explored (5, 6, 10). This approach is practically important because it allows one to tailor the device response for specific material parameters and operating conditions such as concentration. From a fundamental perspective, Sheng et al. have argued (5) that the grating may alter the density of state within the structure, leading to enhancement beyond $4n^2$ over particular frequency ranges. However, the cases we consider here involve shallow gratings on the surface of a thick medium. In such a case, the change of density of state in the structure is substantial only in very limited frequency ranges (25). Instead, our analysis shows that enhancement beyond $4n^2$ is nevertheless achievable because the grating restricts the number of channels available in free space. Also, in refs. 10 and 11, enhancement factors above $4n^2$ were predicted using approximate approaches involving a summation of various scattering events in an incoherent fashion. The analysis presented here is more general in the sense that it is based upon electromagnetic analysis. Moreover, our analysis indicates that the potential of significantly exceeding the conventional limit, defined in terms of $4n^2/\sin^2\theta$, is rather limited in these structures; this conclusion arises because, to achieve high-enhancement factors, one needs to use a periodicity comparable to the wavelength of interest, which leads directly to strong angular and spectral dependency, in consistency with previous results (10). Below, we present a strategy that overcomes these issues and exceeds the conventional limit over a large range of angles and frequencies.

Light-Trapping in Thin Films

When the thickness d of the film is comparable to half wavelength in the material, one can reach the single-mode regime where the film supports a single waveguide mode band for each of the two polarizations. In such a case, Eq. **7** is no longer applicable. Instead, the number of resonances in the frequency range of $[\omega,\omega+\delta\omega]$ can be calculated as (details in *SI Text*)

$$M = 2\times\frac{2\pi n_{wg}^2\omega}{c^2}\left(\frac{L}{2\pi}\right)^2\delta\omega, \quad [11]$$

where the first factor of 2 arises from counting both polarizations. (Here, to facilitate the comparison to the standard conventional limit, for simplicity, we have assumed that the two polarizations have the same group index n_{wg}.) Notice that, in this case, the number of modes no longer explicitly depends upon the thickness d of the film.

In order to highlight the effect of such strong light confinement, we choose the periodicity to be a few wavelengths, in which case the number of channels can still be calculated using Eq. **8**. As a result, we obtain the upper limit for the absorption enhancement factor

$$F = 2\times 4n_{wg}^2\frac{\lambda}{4n_{wg}d}V, \quad [12]$$

where the factor $V = \alpha_{wg}/\alpha_0$ characterizes the overlapping between the profile of the guided mode and the absorptive active layer. The absorption coefficient and group index of the waveguide mode are α_{wg} and n_{wg}, respectively.

Eq. **12** in fact becomes $4n^2$ in a dielectric waveguide of $d \approx \lambda/2n$. Therefore, reaching the single-mode regime is not sufficient to exceed the conventional limit. Instead, to achieve the full benefit of nanophotonics, one must either ensure that the modes exhibit deep-subwavelength-scale electric-field confinement, or enhance the group index to be substantially larger than the refractive index of the active material, over a substantial wavelength range. Below, using both exact numerical simulations and analytic theory, we will design geometries that simultaneously satisfy both these requirements.

Numerical Demonstration

Guided by the theory above, we now numerically demonstrate a nanophotonic scheme with an absorption enhancement factor significantly exceeding the conventional limit. We consider a thin absorbing film with a thickness of 5 nm (Fig. 3*A*), consisting of a material with a refractive index $n_L = \sqrt{2.5}$ and a wavelength-independent absorption length of 25 μm. The film is placed on a mirror that is approximated to be a perfect electric conductor (PEC). A PEC mirror is used for simulation convenience. In practice, it can be replaced by a dielectric cladding layer, which produces similar results (details in *SI Text*). Our aim here is to highlight the essential physics of nanophotonic absorption en-

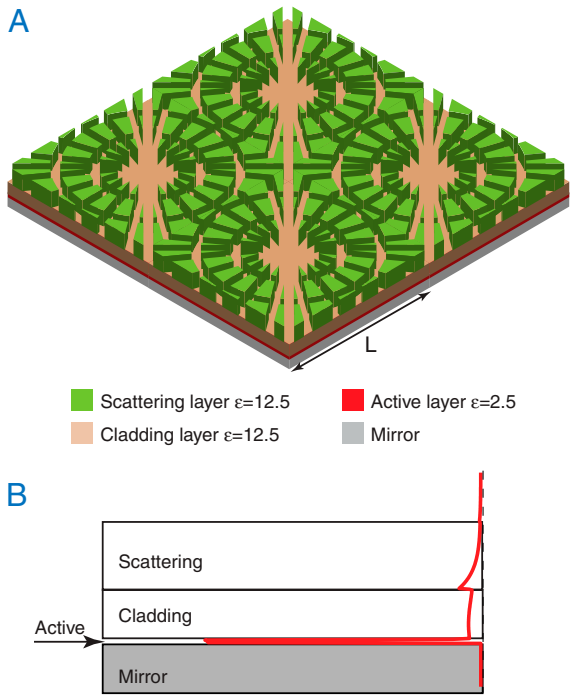

Fig. 3. Structure for overcoming the conventional light-trapping limit. (*A*) A nanophotonic light-trapping structure. The scattering layer consists of a square lattice of air groove patterns with periodicity $L = 1200$ nm. The thicknesses of the scattering, cladding, and active layers are 80, 60, and 5 nm, respectively. The mirror layer is a perfect electric conductor. (*B*) The profile of electric-field intensity for the fundamental waveguide mode. Fields are strongly confined in the active layer. To obtain the waveguide mode profile, the scattering layer is modeled by a uniform slab with an averaged dielectric constant.

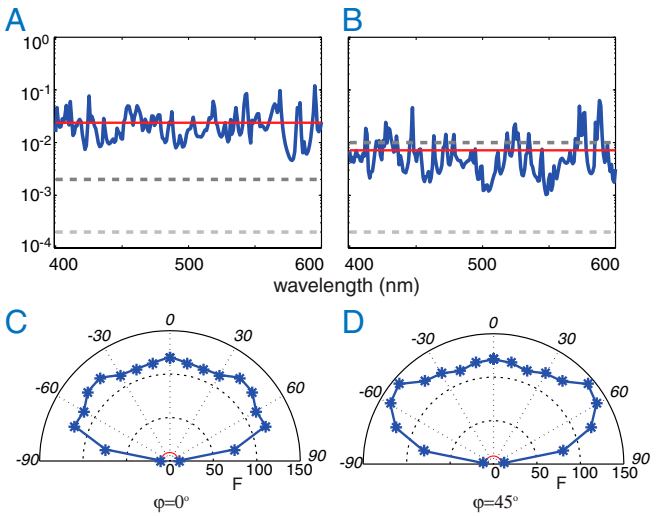

Fig. 4. Absorption with the light-trapping structures. (*A*) Absorption spectrum for normally incident light for the structure shown in Fig. 3. The spectrally averaged absorption (red solid line) is much higher than both the single-pass absorption (light-gray dashed line) and the absorption as predicted by the limit of $4n_L^2$ (dark-gray dashed line). The vertical axis is the absorption coefficient. (*B*) Absorption spectrum without nanoscale light confinement. The structure is the same as that of *A* except that the dielectric constant of the active layer is now the same as the cladding layer. The dark-gray dashed line represents the absorption as predicted by the limit of $4n_H^2$. (*C* and *D*) Angular dependence of the spectrally averaged absorption enhancement factor for the structure in Fig. 3. Incident angles are labeled on top of the semicircles. Incident planes are oriented at 0 (*C*) and 45 (*D*) degrees (azimuthal angles) with respect to the [10] direction of the lattice. The red circles represent the $4n_L^2$ limit.

hancement. The choice of material parameters therefore represents a simplification of actual material response. Nevertheless, we note that both the index and the absorption strength here are characteristic of typical organic photovoltaic absorbers in the weakly absorptive regime (30). Furthermore, there is general interest in using thinner absorbers in organic solar cells given their short exciton diffusion lengths of about 3–10 nm (31–33).

In order to enhance the absorption in the active layer, we place a transparent cladding layer ($n_H = \sqrt{12.5}$) on top of the active layer. Such a cladding layer serves two purposes. First, it enhances density of state. The overall structure supports a fundamental mode with group index n_{wg} close to n_H, which is much higher than that of the absorbing material. Second, the index contrast between active and cladding layer provides nanoscale field confinement. Fig. 3*B* shows the fundamental waveguide mode. The field is highly concentrated in the low-index active layer, due to the well-known slot-waveguide effect (34). Thus, the geometry here allows the creation of a broadband high-index guided mode, with its energy highly concentrated in the active layer, satisfying the requirement in Eq. **12** for high absorption enhancement.

In order to couple incident light into such nanoscale guided modes, we introduce a scattering layer with a periodic pattern on top of the cladding layer, with a periodicity L much larger than our wavelength range of interest. Each unit cell consists of a number of air grooves. These grooves are oriented along different directions to ensure that scattering strength does not strongly depend on the angles and polarizations of the incident light (structure details provided in the *SI Text*). We emphasize that there is no stringent requirement on these grooves as long as the scattering strength dominates over resonance absorption rates.

We simulate the proposed structure by numerically solving Maxwell's equations (Fig. 4*A*; details provided in the *SI Text*). The device has a spectrally averaged absorption enhancement factor of $F = 119$ (red line) for normally incident light. (All the absorption spectra and enhancement factors are obtained by averaging s and p polarized incident light.) Tis enhancement factor is well above the conventional limit for both the active material ($4n_L^2 = 10$) and the cladding material ($4n_H^2 = 50$). Moreover, the angular response is nearly isotropic (Fig. 4 *C* and *D*). Thus such enhancement cannot be attributed to the narrowing of angular range in the emission cone, and instead is due entirely to the nanoscale field confinement effect.

Using our theory, we calculate the theoretical upper limit of light-trapping enhancement in this structure (details in *SI Text*). For wavelength $\lambda = 500$ nm, we obtain an upper limit of $F = 147$. The enhancement factor observed in the simulation is thus consistent with this predicted upper limit. The actual enhancement factor obtained for this structure falls below the calculated theoretical upper limit because some of the resonances are not in the strong overcoupling regime.

To illustrate the importance of nanoscale field confinement enabled by the slot-waveguide effect, we change the index of the material in the absorptive layer to n_H. Such a structure does not exhibit the slot-waveguide effect. The average enhancement in this case is only 37, falling below the conventional limit of 50 (Fig. 4*B*).

Light-Trapping for Infinitesimal Inclusions

The microscopic physics of the enhancement in the numerical example above is related to the Lorentz local field effect (35). In this section, using Eq. **6**, we provide an analytic expression capturing the effect of local field enhancement on light trapping. To obtain a closed-form analytic result, we examine a small inclusion with relevant dimensions at deep-subwavelength scale, of a lossy material with a low index n_L and a small absorption coefficient α_0, embedded in a lossless bulk medium with high index n_H. We study the effect of absorption enhancement when light trapping is performed on the bulk, by, for example, rough-

ening the bulk–air interface (Fig. 5). To facilitate the computation, we assume a periodic boundary condition in the xy plane with a large periodicity L, and a thickness of D for the bulk medium.

To apply Eq. **6**, we first calculate the intrinsic loss rate $\gamma_{i,m}$ of the mth resonance mode having a modal electric field $\vec{E}_m(\vec{r})$:

$$\gamma_{i,m} = \frac{\alpha_0 n_L}{c} \frac{\int_{\text{inclusion}} n_L^2 |\vec{E}_m(\vec{r})|^2 d\vec{r}}{\int n^2(\vec{r}) |\vec{E}_m(\vec{r})|^2 d\vec{r}}. \quad [13]$$

Because the inclusion is small, the field $\vec{E}_m(\vec{r})$ can be derived from a corresponding plane-wave mode in a uniform bulk medium with an electric field $\vec{E}_m(\vec{r}) = \vec{E}_m^0 e^{i\vec{k}_m \cdot \vec{r}}$ having an amplitude $|\vec{E}_m^0| = E_0$. Outside the inclusion region, we assume $\vec{E}_m(\vec{r}) = \vec{E}_m^0(\vec{r})$. The denominator in Eq. **13** thus becomes

$$\int n^2(\vec{r}) |\vec{E}_m(\vec{r})|^2 d\vec{r} \approx n_H^2 E_0^2 L^2 D. \quad [14]$$

Inside the inclusion, the electric fields $\vec{E}_m(\vec{r})$ can be determined by boundary conditions.

We consider the structure in Fig. 5*A* first, where a thin lossy layer perpendicular to the z axis, of a thickness d, is embedded in the high-index bulk. Inside the thin layer, applying the electric-field boundary condition, we have

$$\vec{E}_m(\vec{r}) = E_{x,m}^0(\vec{r})\hat{x} + E_{y,m}^0(\vec{r})\hat{y} + \left(\frac{n_H^2}{n_L^2}\right) E_{z,m}^0(\vec{r})\hat{z}. \quad [15]$$

Combining Eqs. **13–15**, we therefore have

$$\gamma_{i,m} = \frac{\alpha_0 n_L}{c} \frac{n_L^2 (|E_{x,m}^0|^2 + |E_{y,m}^0|^2 + \frac{n_H^2}{n_L^2}|E_{z,m}^0|^2)}{n_H^2 E_0^2} \frac{d}{D}. \quad [16]$$

Thus, the enhancement ratio

$$F = \frac{1}{\alpha_0 d} \cdot \frac{2\pi}{\Delta\omega} \cdot \frac{\sum_m \gamma_{i,m}}{N} = 4n_L^2 \left(\frac{2}{3}\frac{n_H}{n_L} + \frac{1}{3}\frac{n_H^5}{n_L^5}\right). \quad [17]$$

In deriving Eq. **17**, we note that

$$\sum_m |E_{x,m}|^2 = \sum_m |E_{y,m}|^2 = \sum_m |E_{z,m}|^2 = \frac{1}{3} M E_0^2. \quad [18]$$

We also use the relation

$$\frac{2\pi}{\Delta\omega}\frac{M}{N} \cdot \frac{\alpha_0 n_H}{c} = 4n_H^2 \alpha_0 D$$

as derived in a previous section (Eq. **9**).

Eq. **17** is consistent with ref. 36. Our theoretical framework, however, is very general and allows us to treat many other light-trapping scenarios as well. As another example (Fig. 5*B*), we calculate the light-trapping enhancement factor for a small spherical inclusion having a volume V_s embedded in a bulk medium, by noting that inside the sphere, the field is (37)

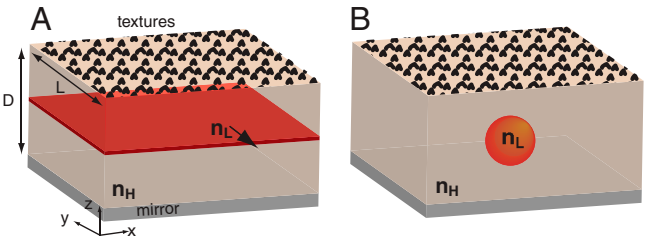

Fig. 5. Illustration of a small active region embedded in a bulk host material: (*A*) a thin layer, and (*B*) a spherical inclusion.

$$|\vec{E}_m(r)| = \frac{3n_H^2}{2n_H^2 + n_L^2} E_0. \quad [19]$$

Following the same procedure as outlined above from the thin-layer case, we have an absorption enhancement factor of

$$F_{\text{sphere}} = 4n_L^2 \frac{9n_H^5/n_L^5}{(2n_H^2/n_L^2 + 1)^2} \quad [20]$$

when compared to the single-pass absorption rate of a sphere of $\alpha V_s/L^2$.

The analytic results thus show that embedding low-index absorptive inclusions in a high-index medium can significantly enhance light absorption beyond the conventional limit, in consistency with the numerical results of the previous section. The combination of wave effects with local field effects may provide significant opportunities for the design of light-absorption enhancement schemes with even higher absorption enhancement factors.

Conclusion

We have developed a statistical coupled-mode theory for nanophotonic light trapping, and have shown that properly designed nanophotonic structures can achieve enhancement factors that far exceed the conventional limit. Our results indicate that substantial opportunities for nanophotonic light trapping exist using only low-loss dielectric components. The basic theory, moreover, is generally applicable to any photonic structure, including nanowire (38, 39) and plasmonic structures (40). In plasmonic structures, the presence of nanoscale guided modes may also provide opportunities to overcome the conventional limit.

ACKNOWLEDGMENTS. The authors thank Eden Rephaeli for providing the simulation code and acknowledge discussions with Jia Zhu, Yi Cui, Peter Peumans, Martin Green, and Eli Yablonovitch. This publication was based on work supported by the Center for Advanced Molecular Photovoltaics (Award KUSC1-015-21), made by King Abdullah University of Science and Technology, and by Department of Energy Grant DE-FG02-07ER46426.

1. Taretto K, Rau U (2004) Modeling extremely thin absorber solar cells for optimized design. *Prog Photovoltaics* 12:573–591.
2. Yablonovitch E (1982) Statistical ray optics. *J Opt Soc Am A* 72:899–907.
3. Goetzberger A (1981) Optical confinement in thin Si-solar cells by diffuse back reflectors. *15th IEEE Photovoltaic Specialists Conference* (Inst of Electrical and Electronics Engineers, New York), pp 867–870.
4. Campbell P, Green MA (1986) The limiting efficiency of silicon solar-cells under concentrated sunlight. *IEEE Trans Electron Dev* 33:234–239.
5. Sheng P, Bloch AN, Stepleman RS (1983) Wavelength-selective absorption enhancement in thin-film solar cells. *Appl Phys Lett* 43:579–581.
6. Bermel P, Luo C, Zeng L, Kimerling LC, Joannopoulos JD (2007) Improving thin-film crystalline silicon solar cell efficiencies with photonic crystals. *Opt Express* 15:16986–17000.
7. Hu L, Chen G (2007) Analysis of optical absorption in silicon nanowire arrays for photovoltaic applications. *Nano Lett* 7:3249–3252.
8. Chutinan A, John S (2008) Light trapping and absorption optimization in certain thin-film photonic crystal architectures. *Phys Rev A* 78:023825.
9. Stuart HR, Hall DG (1997) Thermodynamic limit to light trapping in thin planar structures. *J Opt Soc Am A* 14:3001–3008.
10. Tobias I, Luque A, Marti A (2008) Light intensity enhancement by diffracting structures in solar cells. *J Appl Phys* 104:034502.
11. Saeta PN, Ferry VE, Pacifici D, Munday JN, Atwater HA (2009) How much can guided modes enhance absorption in thin solar cells? *Opt Express* 17:20975–20990.
12. Pala RA, White J, Barnard E, Liu J, Brongersma ML (2009) Design of plasmonic thin-film solar cells with broadband absorption enhancements. *Adv Mater* 21:3504–3509.
13. Mallick SB, Agrawal M, Peumans P (2010) Optimal light trapping in ultra-thin photonic crystal crystalline silicon solar cells. *Opt Express* 18:5691–5706.

14. Lin C, Povinelli ML (2009) Optical absorption enhancement in silicon nanowire arrays with a large lattice constant for photovoltaic applications. *Opt Express* 17:19371–19381.
15. Mokkapati S, Beck FJ, Polman A, Catchpole KR (2009) Designing periodic arrays of metal nanoparticles for light-trapping applications in solar cells. *Appl Phys Lett* 95:053115.
16. Müller J, Rech B, Springer J, Vanecek M (2004) TCO and light trapping in silicon thin film solar cells. *Sol Energy* 77:917–930.
17. Kelzenberg MD, et al. (2010) Enhanced absorption and carrier collection in Si wire arrays for photovoltaic applications. *Nat Mater* 9:239–244.
18. Garnett E, Yang P (2010) Light trapping in silicon nanowire solar cells. *Nano Lett* 10:1082–1087.
19. Pillai S, Catchpole KR, Trupke T, Green MA (2007) Surface plasmon enhanced silicon solar cells. *J Appl Phys* 101:093105.
20. Zeng L, et al. (2006) Efficiency enhancement in Si solar cells by textured photonic crystal back reflector. *Appl Phys Lett* 89:111111.
21. Tsakalakos L, et al. (2007) Silicon nanowire solar cells. *Appl Phys Lett* 81:233117.
22. Rockstuhl C, Lederer F, Bittkau K, Carius R (2007) Light localization at randomly textured surfaces for solar-cell applications. *Appl Phys Lett* 91:171104.
23. Zhu J, et al. (2009) Optical absorption enhancement in amorphous silicon nanowire and nanocone arrays. *Nano Lett* 9:279–282.
24. Anderson PW (1958) Absence of diffusion in certain random lattices. *Phys Rev* 109:1492–1505.
25. Fan S, Joannopoulos JD (2002) Analysis of guided resonances in photonic crystal slabs. *Phys Rev B* 65:235112.
26. Haus HA (1984) *Waves and Fields in Optoelectronics* (Prentice Hall, Englewood Cliffs, NJ), pp 197–234.
27. Fan S, Suh W, Joannopoulos JD (2003) Temporal coupled-mode theory for the Fano resonance in optical resonators. *J Opt Soc Am A* 20:569–572.
28. Kittel C (1995) *Introduction to Solid State Physics* (Wiley, New York), 7th Ed, pp 120–121.
29. Heine C, Morf RH (1995) Submicrometer gratings for solar energy applications. *Appl Opt* 34:2476–2482.
30. Hoppe H, Sariciftci NS (2004) Organic solar cells: An overview. *J Mater Res* 19:1924–1945.
31. Mayer A, Scully S, Hardin B, Rowell M, McGehee M (2007) Polymer-based solar cells. *Mater Today* 10:28–33.
32. Huynh WU, Dittmer JJ, Alivisatos AP (2002) Hybrid nanorod-polymer solar cells. *Science* 295:2425–2427.
33. Yu G, Gao J, Hummelen JC, Wudl F, Heeger AJ (1995) Polymer photovoltaic cells: Enhanced efficiencies via a network of internal donor-acceptor heterojunctions. *Science* 270:1789–1791.
34. Almeida VR, Xu Q, Barrios CA, Lipson M (2004) Guiding and confining light in void nanostructure. *Opt Lett* 29:1209–1211.
35. Aspnes DE (1982) Local-field effects and effective-medium theory: A microscopic perspective. *Am J Phys* 50:704–709.
36. Green MA (2010) Enhanced evanescent mode light trapping in organic solar cells and other low index optoelectronic devices. *Prog Photovoltaics*, in press.
37. Jackson JD (1998) *Classical Electrodynamics* (Wiley, New York), 3rd ed, pp 154–159.
38. Law M, Greene LE, Johnson JC, Saykally R, Yang P (2005) Nanowire dye-sensitized solar cells. *Nat Mater* 4:455–459.
39. Kayes BM, Atwater HA, Lewis NS (2005) Comparison of the device physics principles of planar and radial p-n junction nanorod solar cells. *J Appl Phys* 97:114302.
40. Atwater HA, Polman A (2010) Plasmonics for improved photovoltaic devices. *Nat Mater* 9:205–213.

Supporting Information

Yu et al. 10.1073/pnas.1008296107

SI Text

Reproducing the Standard Conventional Limit for Cells with Nonisotropic Response. This section expands upon the discussion on light trapping in bulk structures, by considering the case where the resonances do not couple to channels isotropically. Suppose the resonances in the structure only couple to light with incident angle less than θ. In applying Eq. **6** to calculate the upper limit for the absorption enhancement factor, we only need to include channels with a radius of $k_{//} = \sin(\theta)\omega/c$ in the $k_{//}$ space:

$$N = \frac{2\pi \sin^2(\theta)\omega^2}{c^2}\left(\frac{L}{2\pi}\right)^2. \qquad [S1]$$

Therefore, the upper limit for the absorption enhancement factor is

$$F = \frac{4n^2}{\sin^2(\theta)}. \qquad [S2]$$

This result agrees with that of ray-optics theory (1, 2).

Analytic Calculation of the Light-Trapping Limit of the Simulated Structure. In this section, we use our theory to calculate the upper limit of the absorption enhancement factor for the structure shown in Fig. 3*A*. The structure in Fig. 3*A* consists of four layers, a top scattering layer, a cladding layer, an active layer, and a mirror plate. In order to determine the upper limit for the absorption enhancement factor, the first step is to calculate the guided mode profiles. For this calculation, we approximate the scattering layer as a uniform layer with its refractive index ($n^2 = 4.64$) determined by averaging the dielectric and air regions. The whole structure supports three waveguide modes at 500 nm wavelength. For each waveguide mode, its loss α_{wg} and group index n_{wg} are calculated directly by mode solving. Its contribution to the upper limit of absorption enhancement factor is then calculated as

$$F = \frac{\alpha_{wg}}{\alpha_0}\frac{\lambda}{d}n_{wg}, \qquad [S3]$$

where the absorption coefficient of the material in the active layer is $\alpha_0 = 400\ \mathrm{cm}^{-1}$, and the thickness of the active layer is $d = 5$ nm. The computations for these modes are summarized in Table S1. It is known that only transverse magnetic (TM) modes have the slot-waveguide effect with the field strongly enhanced in the low-index active layers (3). Here we indeed see significant contributions to the absorption enhancement only from TM modes (Fig. S1). The predicted upper limit, summing over the contributions of all three modes, is 147.

Details of the Simulated Structure. In this section, we provide detailed information about the simulations performed to obtain the absorption spectra for the structures shown in Fig. 3*A*. A scattering-matrix-based numerical simulation was used; details can be found in ref. 4. This method first solves the electromagnetic field in the spatial Fourier space for each layer, and then determines the scattering matrix of the overall structure by matching the boundary conditions between different layers. The number of spatial Fourier components used is 21×21.

The scattering layer has a square lattice with a period $L = 1{,}200$ nm and a thickness of 80 nm. Each unit cell consists of a number of air grooves cutting through the high-dielectric material ($n^2 = 12.5$). There are three sets of air grooves. The first set consists of 10 grooves with width $0.05L$, aligned along the axial direction through the center of the unit cell. These grooves are evenly distributed every 18 deg starting from the [10] direction. The second set consists of two grooves with $0.1L$ width oriented along [11] and [−11] directions. Lastly, two concentric rings ($0.05L$ in width) with radius $0.25L$ and $0.48L$ are introduced to further increase the scattering strength. The scattering layer is then discretized by a 50×50 grid mesh (Fig. S2). Using this mesh, the Fourier components (4) of the dielectric function are calculated by

$$F_{kx,ky} = \frac{1}{2500}\sum_{i,j=1,\ldots,50}\varepsilon(x_i,y_j)e^{-i(k_x x_i + k_y y_j)}.$$

We note that there is in fact no stringent requirement on the design of the scattering pattern, e.g., a wide range of widths and number of air grooves can be used.

Detailed Derivation of Some of the Main Equations in Paper. ***Eq. 2 of the main text: Single resonance absorption spectrum A(ω).*** The amplitudes of resonance and incident channel can be written as

$$a(t) = a(\omega)\exp(j\omega t) \qquad S(t) = S(\omega)\exp(j\omega t), \qquad [S4]$$

where $a(\omega)$ and $S(\omega)$ are spectra of the resonance and incident channel. Substituting into Eq. **1** of the main text, we obtain the spectrum of the resonance amplitude

$$a(\omega) = \frac{j\sqrt{\gamma_e}S(\omega)}{(j(\omega-\omega_0) + (\gamma_i + N\gamma_e)/2}. \qquad [S5]$$

The absorption spectrum can be calculated as

$$A(\omega) = \frac{\gamma_i|a(\omega)|}{|S(\omega)|} = \frac{\gamma_i\gamma_e}{(\omega-\omega_0)^2 + (\gamma_i + N\gamma_e)^2/4}. \qquad [S6]$$

Eq. 7 of the main text: Number of resonant modes M. We consider the photon density of states in a medium that has a thickness d, and a square lattice with a periodicity L. In k space, each resonant mode occupies a volume of $\Delta V_k = \frac{2\pi}{d}\times\frac{2\pi}{L}\times\frac{2\pi}{L}$. The total number of resonances below frequency ω is obtained by counting resonant modes within the sphere specified by radius $k_0 = n\omega/c$:

$$m = 2\times\frac{4\pi}{3}k_0^3\times\frac{1}{\Delta V_k} = \frac{8\pi}{3}\frac{n^3\omega^3}{c^3}\left(\frac{L}{2\pi}\right)^2\frac{d}{2\pi}, \qquad [S7]$$

where the factor of 2 arises from the two polarizations of light. The number of resonances in the frequency range $[\omega,\omega+\delta\omega]$ is then

$$M = \frac{8\pi n^3\omega^2}{c^3}\left(\frac{L}{2\pi}\right)^2\frac{d}{2\pi}\delta\omega. \qquad [S8]$$

Eq. 8 of the main text: Number of channels N. The number of channels is counted in two-dimensional $k_{//}$ space (Fig. 2*A* of the main text). With a period L, each channel takes an area $\frac{2\pi}{L}\times\frac{2\pi}{L}$. All

channels have parallel wavevectors that satisfy $k_{//} < k_0 = \omega/c$. Thus

$$N = 2 \times \pi k_0^2 \times \frac{1}{(2\pi/L)^2} = \frac{2\pi\omega^2}{c^2}\left(\frac{L}{2\pi}\right)^2. \quad \text{[S9]}$$

Again, a factor of 2 arises from two polarizations.

Eq. 10 of the main text: Number of resonances formed by a single waveguide mode. In contrast to Eq. **7**, here the number of resonances is counted in k_{xy} space because there is only one mode in the z direction. The area that each resonance occupies in k_{xy} space is $\frac{2\pi}{L} \times \frac{2\pi}{L}$. The number of resonances below frequency ω is counted within the circle of radius $k_0 = n_{wg}\omega/c$:

$$m = 2 \times \pi k_0^2 \times \frac{1}{(2\pi/L)^2} = 2 \times \frac{\pi n_{wg}^2 \omega^2}{c^2}\left(\frac{L}{2\pi}\right)^2, \quad \text{[S10]}$$

where n_{wg} is the group index of the single mode. For convenience, we assume n_{wg} does not change with frequency and polarization. In the frequency range $[\omega,\omega + \delta\omega]$,

$$M = 2 \times \frac{2\pi {n_{wg}}^2 \omega}{c^2}\left(\frac{L}{2\pi}\right)^2 \delta\omega. \quad \text{[S11]}$$

Absorption Enhancement Without a Perfect Electric Conductor (PEC) Mirror. A PEC mirror is not essential to obtain high light-trapping-based absorption enhancement. Here we consider a structure similar to Fig. 3*A*, except that the PEC mirror is replaced by a dielectric layer with a thickness of 60 nm and a dielectric constant of $n_H = \sqrt{12.5}$ (Fig. S3*A*). The averaged enhancement factor in this case becomes 67 (Fig. S3*B*), which is still well above $4n^2 = 10$. This enhancement factor is about half of the enhancement factor shown in Fig. 4*A* of main text due to the lack of a reflecting mirror.

1. Campbell P, Green MA (1987) Light trapping properties of pyramidally textured surfaces. *J Appl Phys* 62:243–249.
2. Yablonovitch E (1982) Statistical ray optics. *J Opt Soc Am A* 72:899–907.
3. Almeida VR, Xu Q, Barrios CA, Lipson M (2004) Guiding and confining light in void nanostructure. *Opt Lett* 29:1209–1211.
4. Tikhodeev SG, Yablonskii AL, Muljarov EA, Gippius NA, Ishihara T (2002) Quasiguided modes and optical properties of photonic crystal slabs. *Phys Rev B* 66:045102.

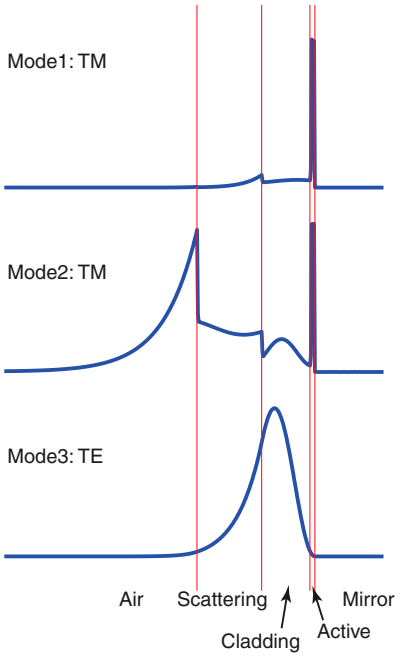

Fig. S1. Profiles of electric-field intensity for the waveguide modes.

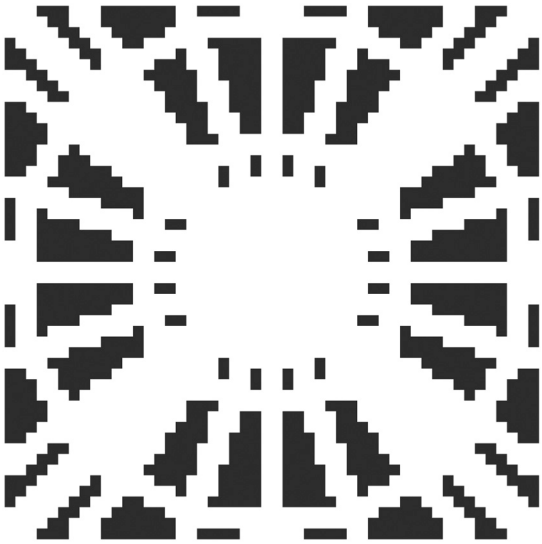

Fig. S2. The real-space pattern of the scattering layer. Black corresponds to high-dielectric regions. White regions are air.

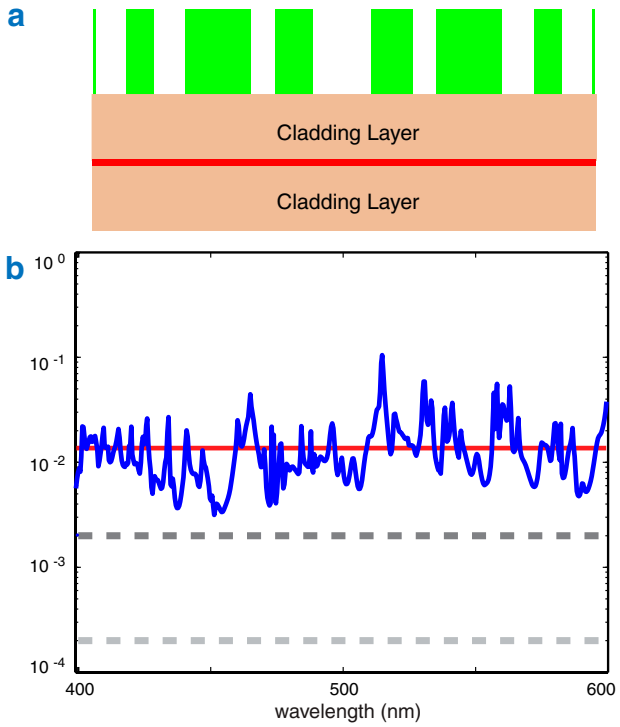

Fig. S3. (*A*) Light-trapping structure where PEC is replaced by a cladding layer. (*B*) Absorption spectrum for the structure shown in *A*.

Table S1. Absorption coefficients and enhancement factor of waveguide modes

Mode	Mode1 TM	Mode2 TM	Mode3 TE
α_{wg}/α_0	0.37	0.069	0.00053
n_{wg}	3.4	3.2	3.9
λ/d ($\lambda = 500$ nm)	100	100	100
Enhancement	125	22	0.2
Total enhancement limit	147.2		

TM, transverse magnetic; TE, transverse electric.